Chinese Journal of Aeronautics, (2022), 35(12): 226–241

Chinese Society of Aeronautics and Astronautics
& Beihang University

Chinese Journal of Aeronautics

cja@buaa.edu.cn
www.sciencedirect.com

Robust optimization of control command for aerospace vehicles with aerodynamic uncertainty

Rui CAO, Yanbin LIU *, Yuping LU

College of Automated Engineering, Nanjing University of Aeronautics and Astronautics, Nanjing 210016, China

Received 21 June 2021; revised 13 August 2021; accepted 18 October 2021
Available online 25 January 2022

KEYWORDS

Aerospace vehicle;
Multi-objective optimization;
Polynomial chaos;
Uncertain systems

Abstract To reduce the design burden of Aerospace Vehicles (ASVs) control systems, this paper proposes a multi-constrained robust trajectory optimization method, which provides a good front-end input for the control system. Differ from the conventional aircraft, some control performance of ASVs is not only related to the model parameters, but also affected by the flight status. Therefore, the robust optimization method combines this characteristic of ASVs, sets the control performance as one of the optimization objectives, and considers the influence of parameter uncertainty. In this method, the polynomial chaos expansion algorithm is used to transform the trajectory optimization problem with uncertain parameters into the equivalent deterministic robust trajectory optimization problem. Finally, compared with traditional deterministic trajectory optimization methods to illustrate the effectiveness of proposed control optimization method.

1. Introduction

Aerospace Vehicles (ASVs) have broad application prospects and strong research needs, in which hypersonic flight is one of the main defense and space exploration technologies.[1] This type of vehicle is designed to operate under larger flight envelopes, thus a Turbine-Based Combined Cycle (TBCC) engine is required to fly through these different speed ranges.[1,2] At present, researchers hope to ensure that the ASVs have good control performance in a large flight range by the control system.[3] However, the special layout of the fuselage/propulsion integration and the small actuator margin increases its control complexity.[4] In addition, the wide flight range and uncertainty continue raising the burden on the control system. If only relying on the control system to overcome all the problems and achieve the desired goals, for the control system is extremely difficult or even impossible. According to the Refs. 5,6, some control performance of ASV is not only related to the model parameters, but also affected by the flight status. Therefore, the control performance and aerodynamic parameter uncertainty can be considered in advance in the trajectory design stage. Subsequently, the optimization result can be used as the reference control input to the actual control system. In other words, it provides a good front-end input to reduce the control burden, which is of great value for dealing with actual aircraft engineering problems.

Uncertainties faced by aircraft are usually solved by the control system,[7] the trajectory design only considers the nom-

* Corresponding author.
E-mail address: nuaa_liuyanbin@139.com (Y. LIU).
Peer review under responsibility of Editorial Committee of CJA.

Production and hosting by Elsevier

https://doi.org/10.1016/j.cja.2022.01.011

inal state.[8,9] However, this work will deal with the influence of some uncertain factors in the trajectory design stage, to balance the burden of trajectory planning and control system design, which is a promising trajectory optimization idea. In this study, uncertainty modeling and propagation are key steps. For nonlinear dynamic systems, Monte Carlo (MC),[10] Markov chain,[11] unscented transform,[12] Fokker-Planck-Kolmogorov framework,[13] and Polynomial Chaos (PC)[14] can be used to quantify the uncertainty caused by uncertain variables. The MC method is popular because of its ease of implementation, but its computational cost precludes its application in robust optimization. Recently, the PC method has gained much attention since it can provide accuracy comparable to the MC method at a significantly lower computational cost. Methods based on PC Expansions (PCE) have been applied to various disciplines in aerospace engineering, including aerodynamics,[15] airfoil design,[16] coupled aerodynamics-structure analysis,[17,18] and flight dynamics.[14,19,20]

In the field of aerospace engineering, the study of stochastic dynamic systems mainly focuses on effective algorithms for uncertainty propagation.[14,19,20] Only a few studies on optimization design of uncertain dynamic system, which can be found in Ref. 21 and Ref. 22. With the emphasis on trajectory robust optimization problems, the research on this aspect increases. Ref. 23 and Ref. 24 used the PCE method to transform the original stochastic trajectory optimization problem into an equivalent deterministic one in the expanded higher-dimensional state space, then adopted the pseudo-spectral method to optimize the augmented deterministic system to obtain a robust optimized trajectory. In Ref. 25 and Ref. 26, the non-intrusive PCE scheme was employed to optimize the airplane trajectory with uncertain aerodynamic parameters. Jin et al.[27] combined the genetic algorithm and the MC method to solve the uncertain rendezvous and proximity operations in perturbed elliptical orbits. Ref. 12 and Ref. 28 were based on the unscented transformation method to solve the stochastic ascent trajectory optimization problem for a two-stage, semi-reusable space launch system. Grant and Bolender[29] proposed the higher-order stress cases to capture the worst-on-worst set of dispersions obtained by MC simulation, and achieved robust optimization by optimizing the worst-case scenarios. Flanzer et al.[30] used mutually orthogonal random uncertain parameter combinations on nested sparse grids to calculate trajectories, and then obtained the mean and variance of these trajectories to perform robust optimization. Richter and Holzapfel[31] designed stochastic collocation to obtain the mean and standard deviation of uncertain state, then used the pseudo-spectral method to minimize the statistical information to calculate the best flight trajectory.

In the research of robust trajectory optimization by the aforesaid researchers, the oriented system is a 3 Degree-of-Freedom (DOF) point-mass model instead of the 6DOF model used in actual flight control. In the trajectory optimization problems based on 3DOF point-mass model, the Angle-of-Attack (AOA) is often the control variable. If the optimal AOA history is without the reasonable boundary and variation rate, then the controller is difficult to track the desired trajectory. This leads to the question that whether the resulted optimal trajectory is actually controllable. In addition, 3DoF trajectory optimization is difficult to set the control performance as one of the optimization objects, because it cannot provide the transfer function of the elevator to the angle of attack/pitch rate. To solve these problems, we have carried out the work of this article. Considering the multiple constraints and uncertainties of ASVs, based on the 6DOF longitudinal model, a multi-constraint robust trajectory optimization method is proposed. Moreover, the optimization method takes some control performance as one of the trajectory optimization objectives to ensure that the aircraft still has good performance under the uncertain aerodynamic parameters. Thus, the optimal trajectory obtained by this method has good robustness and control performance under open-loop conditions.

The remainder of this paper is organized as follows: In Section 2, the kinematics model and dynamic analysis of ASV are introduced. In addition, a deterministic trajectory optimization problem considering control constraints is proposed. Subsequently, an implementable computational model of robust control command optimization for uncertain systems is presented in Section 3. In Section 4, the effectiveness of augmented system based on PCE to describe the uncertain system is analyzed. Furthermore, the designed robust optimization method and the conventional optimization ideas[9] are respectively applied to the ASV nonlinear system to verify the effectiveness of designed method in this article. Section 5 concludes the paper.

2. Problem statements

2.1. Model analysis of aerospace vehicle

This paper takes the Generic Hypersonic Aerodynamics Model Example (GHAME) vehicle as the research object[32] for subsequent analysis and simulation. The outline layout of GHAME is shown in Fig. 1. The longitudinal dynamics of ASVs can be described as the following nonlinear differential equations:

$$\dot{r} = V\cos c \tag{1a}$$

$$\dot{h} = V\sin c \tag{1b}$$

$$\dot{V} = \frac{T\cos a - D}{m_{vehicle}} - \frac{l_g \sin c}{r_g^2} \tag{1c}$$

$$\dot{c} = \frac{T\sin a + L}{m_{vehicle} V} - \frac{\left(l_g - V^2 r_g\right)\cos c}{V r_g^2} \tag{1d}$$

$$\dot{a} = q - \dot{c} \tag{1e}$$

$$\dot{q} = M/I_y \tag{1f}$$

$$\dot{m}_{vehicle} = \frac{-T}{g_0 I_{sp}} \tag{1g}$$

where V, c, a, q denote the flight speed, flight-path angle, AOA and pitch angle rate, respectively. r and h represent horizontal displacement and altitude of ASV. $m_{vehicle}$ indicates the vehicle weight and I_y is the inertia moment. I_{sp} denotes the specific impulse. $\dot{m}_{vehicle}$ is the fuel mass flow rate. g_0 is the gravitational acceleration of the earth surface. l_g expresses the gravitational constant, r_g is the earth radius. L, D, T and M represent lift, drag, thrust and pitching moment of GHAME, respectively.

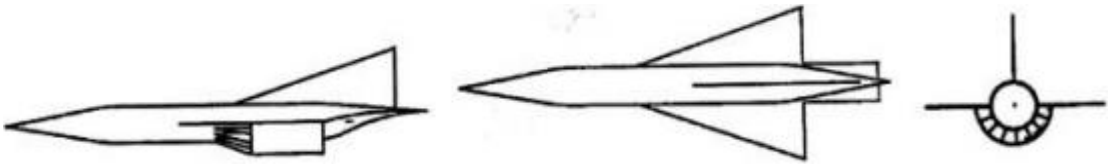

Fig. 1 GHAME vehicle configuration.[32]

Similarly to what was done in Oscar et al.,[33] approximations of the forces and moments to be employed for trajectory design have been derived as follows:

$$\begin{cases} L = \bar{q}\,S_{ref}\left[C_{L0} + C_L^{Ma}Ma + C_L^{Ma^2}Ma^2 + C_L^{a}a + C_L^{a\cdot Ma}(a\cdot Ma) + C_L^{a\cdot Ma^2}(a\cdot Ma^2) + C_L^{d_e}d_e\right] \\ D = \bar{q}\,S_{ref}[C_{D0} + C_D^{Ma}Ma + C_D^{Ma^2}Ma^2 + C_D^{Ma^3}Ma^3 + C_D^{a}a + C_D^{a^2}a^2 + C_L^{a\cdot Ma}(a\cdot Ma) \\ \quad + C_L^{a\cdot Ma^2}(a\cdot Ma^2) + C_L^{a^2\cdot Ma}(a^2\cdot Ma)] \\ M = \bar{q}\,S_{ref}\left[C_{M0} + C_M^{Ma}Ma + C_M^{a}a + C_L^{a\cdot Ma}(a\cdot Ma) + C_M^{d_e}d_e\right] \end{cases} \tag{2}$$

where

$$C_L^{d_e} = C_{Le}^0 + C_{Le}^a a + C_{Le}^{Ma}Ma + C_{Le}^{Ma^2}Ma^2$$
$$C_M^{d_e} = C_{Me}^0 + C_{Me}^a a + C_{Me}^{Ma}Ma + C_{Me}^{a\cdot Ma}(a\cdot Ma)$$

d_e represents elevator deflection, Ma is the Mach number, $\bar{q}$ denotes dynamic pressure, and S_{ref} expresses the vehicle reference area.

The engine model is shown in Eq. (3).[34] The fuel/air ratio of engine is adjusted to stoichiometric ratio, which is $0{:}029\,/_F$. Thrust T is a function of the Fuel Equivalent Ratio (FER), AOA, and Mach number

$$T = 0{:}029\,/_F I_{sp}(Ma;\,/_F)qg_0VC_T(Ma;a)A_c \tag{3}$$

where $/_F$ is the FER, q denotes the atmospheric density, A_c represents the inlet airflow capture area. The expressions of I_{sp} and capture-area coefficient C_T are as follows:

$$C_T = C_{T0} + C_T^a a + C_T^{a^2}a^2 + C_T^{Ma}\lg(Ma) + C_T^{a\cdot Ma}(a\cdot\lg(Ma)) + C_T^{a^2\cdot Ma}(a^2\cdot\lg(Ma))$$
$$I_{sp} = I_0 + I_1\frac{1}{\sqrt{/_F}} + I_2\frac{1}{/_F} + I_3Ma + I_4Ma\cdot\lg(Ma) + I_5Ma^{3=2} + I_6Ma^2 + I_7Ma^2\cdot\lg(Ma)$$

The ranges of the above aerodynamic and propulsion coefficients are at the flight conditions with Mach number $Ma \in [0{:}4;\ 24]$ and angle of attack of $a \in [-3^o;\ 21^o]$.

2.1.1. Model constraints

Due to the complex structure and flight environment, the actuators and flight status of ASVs would be more restricted. The main constraints are shown in Eq. (4). Here, the upper bound constraint of AOA is mainly restricted by the condition of inlet unstart. FER is subject to a state-dependent constraint, which defines the operability of the scramjet engine. The remaining control input d_e is restrained by the physical limitations in the elevator deflection.

$$d_{e;min} \leq d_e \leq d_{e;max} \tag{4a}$$

$$/_{F;min} \leq /_F \leq /_{F;chock}(a;\bar{q};Ma) \tag{4b}$$

$$a_{min} \leq a \leq G_a(Ma) \tag{4c}$$

where $d_{e;max}$, $/_{F;chock}(a;\bar{q};Ma)$, $G_a(Ma)$ and $d_{e;min}$, $/_{F;min}$, a_{min} are the upper and lower bounds of the control variables and AOA, respectively. The FER fitting expression which causes the engine choke (denoted as $/_{F;chock}$) is given in Ref. 34, as shown in Eq. (5).

$$\begin{aligned} /_{F;chock} &= c_0 + c_1Ma + c_2Ma^2 + c_3Ma^3 + c_4a + c_5a^2 + c_6a^3 + c_7\bar{q} + c_8\bar{q}^2 + c_9\bar{q}^3 \\ &+ c_{10}(a\cdot Ma) + c_{11}(\bar{q}\cdot Ma) + c_{12}(a^2\cdot Ma^2) + c_{13}(\bar{q}^2\cdot Ma^2) + c_{15}(a^2\cdot\bar{q}^2) \\ &+ c_{16}(a^2\cdot Ma) + c_{17}(\bar{q}^2\cdot Ma) + c_{18}(a\cdot Ma^2) + c_{19}(\bar{q}\cdot Ma^2) + c_{20}(a\cdot\bar{q}^2) + c_{21}(a^2\cdot\bar{q}) \end{aligned} \tag{5}$$

where the coefficients for $/_{F;chock}$ can be referred to Ref. 34.

Fig. 2 shows that the variation of back pressure ratio with a at different Ma, which gives the AOA boundary of the hypersonic inlet unstart.[35] The boundary is numerically fitted to obtain the AOA constraint as shown in Eq. (6).

$$G_a(Ma) = G_0 + G_1Ma + G_2Ma^2 + G_3Ma^3 \tag{6}$$

According to Eqs. (5)–(6), it can be seen that FER is affected by AOA, and the AOA is also limited by the engine state. Meanwhile, the engine inlet pressure would cause the pitch moment change, thereby affecting the AOA. This shows that there is a coupling effect between the AOA and the FER, which makes the constraint relationship of ASV more complex. In addition, due to the aerodynamic coefficient uncertainty, the constraint boundary would be more unclear, which further increases the design difficulty of the control system.

2.1.2. Hypersonic model analysis

ASVs not only have the complex nonlinearity and constraint that conventional aircraft do not, but also possess different longitudinal motion characteristics. This unique flight characteristic may contribute to the trajectory planning and controller design of ASVs.

According to Ref. 2, different from the low-speed flight, although the angle of attack is a short-period state during high-speed flight, it also is affected by long-period motion state (such as flight speed, altitude). In other words, in the case of high-speed flight, the velocity and altitude of vehicle will affect the angle of attack motion. Moreover, for ASVs, the aerodynamic derivatives are no longer constants, and the variation

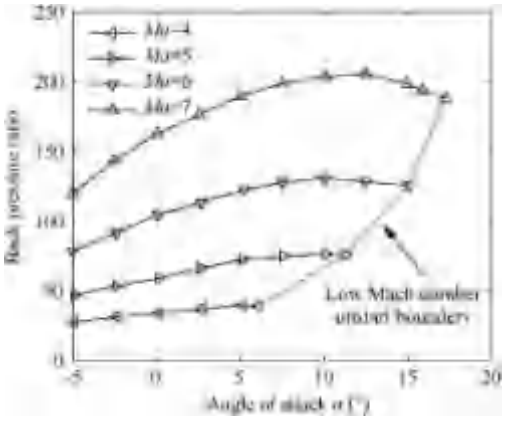

Fig. 2 Effects of Ma and a on back pressure ratio.

of atmospheric density cannot be ignored. Therefore, the flight performance of ASVs is not only related to model parameters, but also affected by flight trajectory/status.[5,6] And Ref. 7 also illustrates this.

Based on the above contents and the conclusions of related researchers, the relationship between control performance, aerodynamic parameter, and flight trajectory is summarized, as shown in Fig. 3.

According to Fig. 3, the variation of aerodynamic parameter would affect the nominal trajectory, then the change of Mach number and dynamic pressure caused by the trajectory would also impact the current aerodynamic coefficient. Moreover, the aerodynamic derivatives (@C_M=@a(V); @T=@h; @T=@V, etc.) related to the control performance are correlated with the flight speed and altitude, so they are also affected by the flight trajectory changes. Therefore, the coupling relationship of ASVs may bring about the complexity of controller design. However, from another perspective, it gives a hint that trajectory can affect some control performance of ASVs.

To have a more intuitive display, the influence of flight trajectory on Short-period Damping-Frequency (SDF) characteristic of ASVs is analyzed. Considering that the vehicle climbs along with the constant dynamic pressure in the range of 30 kPa-120 kPa, and then several points on each isodynamic pressure trajectory are selected to analyze the corresponding SDF characteristic. Fig. 4 shows the distribution of SDF characteristic on different dynamic pressure trajectories. Among them, the relevant levels (Level one, Level two, etc.) are divided according to the flight quality manual.[36]

According to Fig. 4, it can be seen that this characteristic of ASVs would change with the flight Mach number and dynamic pressure (or altitude). Therefore, it is reasonable to consider this feature in the trajectory optimization objective. In other words, the control performance greatly affected by the trajectory can be regarded as one of the objective functions for trajectory optimization. On this basis, this work improves the traditional optimization problem, so that some control performance is considered in the trajectory design stage.

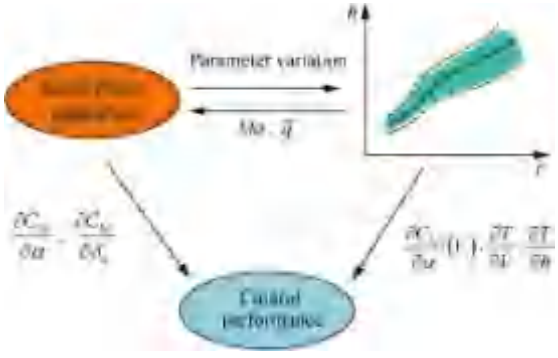

Fig. 3 Diagram of influence relationship.

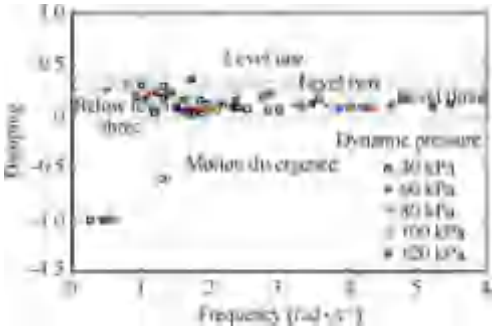

Fig. 4 Short-period damping-frequency distribution diagram of GHAME along the trajectory.

2.2. Trajectory optimization problem of ascent phase

2.2.1. Traditional trajectory optimization problem

The general form of a deterministic dynamic problem, which can be written as follows [25]. Find u(t), makes

$$\begin{aligned} &\text{Min } J = U(x(t_0);u(t_0);x(t_f);u(t_f);t_f) + \int_{t_0}^{t_f} W(x(t);u(t);t)dt \\ &\text{Subject to} \\ &\dot{x}(t) = f(x(t);u(t);t) \\ &C(x(t);u(t);t) \le 0 \\ &H(x(t_0);u(t_0);x(t_f);u(t_f);t_f) = 0 \end{aligned} \tag{7}$$

where t is the time, x denotes the state vector, u(t) represents the design variable, $C \in R^{n_C}$ is the path constraint, and $H \in R^{n_H}$ is the boundary constraint. $U(\cdot)$ represents the terminal optimization form, $\int_{t_0}^{t_f} W(\cdot)dt$ represents the integral optimization form. Generally, the design variable u in optimization problem (7) is AOA. Moreover, the performance index J is the shortest time, the minimum fuel consumption and so on, does not involve the control performance.

2.2.2. Trajectory optimization problem considering control performance

Different from the conventional optimization problem (7) using AOA as a design variable, d_e and $/_F$ are taken as design variables in the trajectory optimization method proposed in this paper. Hence, it can provide the corresponding reference control input for the actual controller, and also lay the foundation for introducing control performance into the trajectory optimization problem.

Since the aerospace vehicle is usually designed to be statically unstable, short-period performance (damping-frequency characteristics) must be guaranteed first in control. In addition, compared with anti-interference performance, tracking performance, and control feasible region, the SDF characteristic is more affected by trajectory. Therefore, in the trajectory optimization method of this paper, this control performance - the SDF characteristic is mainly considered as one of the optimization objectives. The short-period ideal model with a level-one Flying Quality (FQ)[36] is shown below:

$$\frac{h(s)}{d_e(s)} = \frac{K_q(s + 1/T_{h2})}{s^2 + 2f_{sp}x_{sp}s + x_{sp}^2} \tag{8}$$

where s indicates differential operator, $K_q = 1$, $T_{h2} = 0{:}7143$, $f_{sp} = 0{:}707$, $x_{sp} = 3{:}5$. $\dot{h} \equiv q$ is the pitch angle rate, f_{sp} and x_{sp} are the damping ratio and natural frequency.

Ref. 36 gives a function to measure the similarity of two systems in the frequency-domain, namely the mismatch function. The smaller the value of mismatch function is, the higher the similarity between the two systems is. Therefore, based on this concept, Eq. (9) is given to measure the similarity of frequency-domain characteristics between complex high-order systems and ideal model (8) with level-one FQ, so as to indirectly estimate the SDF characteristic of ASVs.

The smaller the value of Eq. (9), the higher the similarity between the two systems, which means that the frequency domain characteristics of complex systems are closer to the ideal model (8), that is, its SDF characteristic are better (closer to the level-one FQ) under open-loop. Consequently, the SDF characteristic can be introduced into the optimization objective by minimizing Eq. (9).

$$J_{SDF} = \sum_{x_i} [G_H(x_i) - G_S(x_i)]^2 + K[P_H(x_i) - P_S(x_i)]^2 \tag{9}$$

where G and P correspond to the amplitude and phase of systems. x_i is the frequency of interest and is chosen within the range $[1;\ 10]$rad=s in this paper. The subscript H denotes the complex system, the subscript S represents the ideal model (8), and K indicates the weighting factor, which is chosen as 0.01745.[2,5,36]

In addition, the target position and the fuel consumption are also considered. Then, the optimization objective is to minimize the errors between terminal position $(r_f; h_f)$ and target position $(r_T; h_T)$, the fuel consumption, and the J_{SDF}, namely:

$$J_0 = \min\{ j_1 d_{mass} + j_2(\| r_f - r_T \|_2 + \| h_f - h_T \|_2) + j_3 J_{SDF} \} \tag{10}$$

where $d_{mass} = m_{vehicle}(t_0) - m_{vehicle}(t_f)$, the subscript f represents the terminal state of variable. j_1, j_2 and j_3 are the weight, which are set by the user.

The next stage of ascent phase is the cruise phase or the separation window of the two-stage to orbit vehicle. This means that the terminal state of ascent phase is also the initial state of cruise phase or separation window. Therefore, it is necessary to set the terminal constraints of ascent phase according to the predetermined mission requirements. In general, the following constraint inequalities are adopted:

$$|dV_f| \leq dV_{f;max};\ |dh_f| \leq dh_{f;max};\ |dr_f| \leq dr_{f;max} \tag{11}$$

where $|dV_f|$, $|dh_f|$, and $|dr_f|$ are the errors of velocity, height, and horizontal displacement between the terminal and the target, respectively. $dV_{f;max}$, $dh_{f;max}$, and $dr_{f;max}$ are the corresponding allowable error thresholds.

According to the previous discussion, the trajectory optimization problem of ascent phase in this paper can be expressed as the following Optimal Control Problem (OCP):

$$\begin{aligned} &\text{find} && d_e(t) \text{ and } /_F(t) \\ &\quad \min && (10) \\ &\text{s:t:} && \text{Eqs: } (1); (4); (11) \end{aligned} \tag{12}$$

Remark: Problem (12) belongs to the deterministic trajectory optimization problem, that is, the influence of parameter disturbance or initial value uncertainty on the resulted trajectory is not considered.

Under this optimization result obtained by solving the problem (12), once the aerospace vehicle is affected by uncertain perturbation or interference, it will easily deviate from the pre-designed optimized trajectory and be difficult to satisfy the expected constraints. If the influence of parameter uncertainty is considered in trajectory optimization, the resulted nominal trajectory has good robustness to the uncertainty. Furthermore, it can provide a feedforward input with better performance to the controller, thus balancing the burden of trajectory planning and control system design.

Consequently, in the next section, the PCE method is introduced to quantify the uncertainty of system and constraint, so as to update the deterministic optimization problem (12) to the robust optimization problem considering control performance. Finally, this optimization problem is solved to complete the robust optimization design of ascent trajectory.

3. Robust optimization scheme for ASVs

In this section, based on the PCE method, the process of converting an uncertain dynamic system into an equivalent deterministic dynamic system in an expanded higher-dimensional state space is introduced. Besides, a robust control command optimization method is proposed.

3.1. The quantification process of uncertain system

3.1.1. Equivalent deterministic differential equations based on PCE

Considering that the aerodynamic of GHAME has uncertain information D:

$$\begin{aligned} &L = (1 + d_L \mathsf{D})\,\bar{L};\ D = (1 + d_D \mathsf{D})\,\bar{D}; \\ &M = (1 + d_M \mathsf{D})\,\bar{M};\ T = (1 + d_T \mathsf{D})\,\bar{T} \end{aligned} \tag{13}$$

where the random variable $\mathsf{D} \in [-1; 1]^d$, d is the dimension of D. d_L, d_D, d_M, d_T represent the perturbations with regard to the corresponding nominal values $\bar{L}$, $\bar{D}$, $\bar{M}$, $\bar{T}$, respectively. Therefore, Eq. (1) is transformed into Random Differential Equations (RDEs):

$$\dot{\mathsf{x}} = f(t; \mathsf{x}; \mathsf{D}) \tag{14}$$

where t represents the system time, $\mathsf{x} = [r; h; V; c; a; q; m_{vehicle}] \in R^n$, and n is the state dimension of system (1), equal to seven.

The solution of Eq. (14) is a random process closely related to the random variable D. Then, based on the PCE method, the state variable under the influence of D can be expanded, and the following formula is obtained.

$$\hat{\mathsf{x}}_l(t; \mathsf{D}) = \sum_{j=0}^{N_p} \hat{\mathsf{x}}_{lj}(t)\, u_j(\mathsf{D}); \quad l = 1; 2; \ldots; n \tag{15}$$

$$\hat{\mathsf{x}}_{lj}(t) = \int \hat{\mathsf{x}}_l(t; \mathsf{D})\, u_j(\mathsf{D}) q(\mathsf{D}) d\mathsf{D} \tag{16}$$

where $\hat{\mathsf{x}}_l$ represents the approximate value of lth state, and $N_p = (p + d)!\ =p!d! - 1$, p is the order of expansion polynomial. $\hat{\mathsf{x}}_{lj}$ denotes the jth orthogonal basis coefficient corresponding to x_l. $u_j(\mathsf{D})$ indicates the jth orthogonal polynomial

related to the random variable D. $q(\mathsf{D})$ is regarded as the Probability Density Function (PDF) of random variable.

Considering that the random variable D obeys uniform distribution, Eq. (15) is substituted into Eq. (14), and its projection on the basis function is obtained via the Galerkin method, to generate the Deterministic Differential Equations (DDEs) corresponding to Eq. (14). This process can refer to our previous research work.[37] Due to the excessive relevant content and the space limitation of paper, the specific process is not carried out in detail. The equivalent DDEs obtained by PCE are as follows:

$$\dot{r}_s = \frac{1}{\langle u_s^2\rangle}\sum_{j=0}^{N_p} V_j\left\langle u_s u_j \cos\left(\sum_{j=0}^{N_p} c_j u_j\right)\right\rangle \tag{17a}$$

$$\dot{h}_s = \frac{1}{\langle u_s^2\rangle}\sum_{j=0}^{N_p} V_j\left\langle u_s u_j \sin\left(\sum_{j=0}^{N_p} c_j u_j\right)\right\rangle \tag{17b}$$

$$\begin{aligned}\dot{V}_s = {} & \frac{1}{\langle u_s^2\rangle} \\ & \times \sum_{i=0}^{N_p}\left\langle \frac{\left(T_i u_i \cos\left(\sum_{j=0}^{N_p} a_j u_j\right) - \sum_{k=0}^{N_p} D_k u_k\right)}{\sum_{j=0}^{N_p} m_{\text{vehicle};j} u_j} u_s\right\rangle \\ & - \frac{l_g}{r_g^2}\frac{1}{\langle u_s^2\rangle}\left\langle \sin\left(\sum_{j=0}^{N_p} c_j u_j\right) u_s\right\rangle\end{aligned} \tag{17c}$$

$$\begin{aligned}\dot{c}_s = {} & \frac{1}{\langle u_s^2\rangle}\sum_{i=0}^{N_p}\left\langle \frac{T_i u_i \sin\sum_{j=0}^{N_p} a_j u_j + \sum_{k=0}^{N_p} L_k u_k}{\sum_{j=0}^{N_p} m_{\text{vehicle};j} u_j \cdot \sum_{l=0}^{N_p} V_l u_l} u_s\right\rangle \\ & - \frac{l_g}{r_g\langle u_s^2\rangle}\left\langle \cos\left(\sum_{i=0}^{N_p} c_j u_j\right)\left(\sum_{i=0}^{N_p} V_i u_i\right)^{-1} u_s\right\rangle \\ & + \frac{1}{r_g\langle u_s^2\rangle}\sum_{i=0}^{N_p}\left\langle V_i u_i \cos\left(\sum_{j=0}^{N_p} c_j u_j\right) u_s\right\rangle\end{aligned} \tag{17d}$$

$$\dot{a}_s = \frac{1}{\langle u_s^2\rangle}\left\langle \sum_{j=0}^{N_p} q_j u_j u_s\right\rangle - \dot{c}_s \tag{17e}$$

$$\dot{q}_s = \frac{1}{I_y\langle u_s^2\rangle}\sum_{j=0}^{N_p}\langle M_j u_j u_s\rangle \tag{17f}$$

$$\dot{m}_{\text{vehicle};s} = \frac{-1}{g_0 I_{sp}\langle u_s^2\rangle}\sum_{j=0}^{N_p}\langle T_j u_j u_s\rangle \tag{17g}$$

where $s = 0; 1; \cdots; N_p$, and $\langle\cdot\rangle$ is the mean operator. $r_i; h_i; V_i; c_i; a_i; q_i; m_{\text{vehicle};i}$; $i = 0; 1; \cdots; N_p$ are the polynomial chaos coefficients of stochastic state variables $r(\mathsf{D}); h(\mathsf{D}); V(\mathsf{D}); c(\mathsf{D}); a(\mathsf{D}); q(\mathsf{D}); m_{\text{vehicle}}(\mathsf{D})$, respectively. Then, the stochastic dynamical system (14) in R^n is transformed into deterministic dynamical system in $R^{n(N_p+1)}$. Therefore, the solutions of DDEs in Eq. (17) can be employed to characterize the flight states with uncertainties.

3.1.2. Correction of equivalent DDEs

Since the RDEs of ASVs are highly nonlinear, the long-term integration of polynomial (17) would cause the variation of random characteristics.[38] This will make the original basis family of random variables loses its representativeness, resulting in algorithm divergence.

To solve the divergence of PCE algorithm caused by the nonlinearity of ASVs, an adaptive polynomial chaos algorithm is proposed to update DDEs adaptively. In this algorithm, the Spectral Decomposition (SD) technology[39] is introduced to consider the change of the random characteristics of system state. Moreover, to perceive the significant changes of stochastic features (i.e. the original basis family is no longer applicable), the truncation error is used as an indicator[40]. The algorithm will adaptively updated the basis family, whenever the truncation error exceeds the threshold, to suppress divergence and improve the accuracy of PCE. The trigger conditions of updating the orthogonal basis are as follows[40]:

$$\max_{j=2;3;\ldots;N_p}\left|\hat{x}_{lj}(t)\right| \;\mathsf{P}\; \mathbb{m}_l\left|\hat{x}_{l1}(t)\right|;\; l = 1; 2; \ldots; n \tag{18}$$

where $\hat{x}_{lj}(t)$ is the jth PCE coefficient of lth random state at time t, which is calculated by Eq. (16). $\mathbb{m}_l$; $l = 1; 2; \ldots; n$ are the selected tolerance coefficients. If any one of states satisfies the above condition at $t = t_1$, new random variables need to be introduced as new orthogonal basis. According to Ref. 40, this new random variable is equal to the solution of $\hat{x}_l(t)$ at $t = t_1$, given by

$$\acute{}_l = \hat{x}_l(t_1; \mathsf{D}) = \sum_{j=0}^{N_p}\hat{x}_{lj}\,u_j(\mathsf{D}) = Z_l(\mathsf{D});\quad l = 1; 2; \ldots; n \tag{19}$$

where Z_l maps D onto $\acute{}_l$. This mapping is not necessarily bijective. The PDF of D is $q(\mathsf{D})$, then the PDF $q_{\acute{}_l}(\acute{}_l)$ of $\acute{}_l$ can in principle be obtained from[40]

$$q_{\acute{}_l}(\acute{}_l) = \sum_k \frac{q(\mathsf{D}_k)}{\left|\frac{dZ_l(\mathsf{D})}{d\mathsf{D}_k}\right|} \tag{20}$$

where $\mathsf{D}_k(k = 1; 2; \cdots)$ denotes all roots of $\acute{}_l - Z_l(\mathsf{D}) = 0$. After obtaining the new PDF about $\acute{}_l$, the orthogonal basis family $/(\acute{}_l)$ corresponding to the random variable $\acute{}_l$ can be established by applying the Schmidt orthogonalization rule. In this way, the PCE of random state variables can be updated as follows

$$\hat{x}_l(t; \acute{}_1; \acute{}_2; \cdots \acute{}_n) = \sum_{0 \mathsf{6} k_1+k_2\cdots+k_{n-1} \mathsf{6} N_p} x_{l;k_1k_2\cdots k_{n-1}}(t)/_{k_1}(\acute{}_1)/_{k_2}(\acute{}_2)\cdots/_{k_n}(\acute{}_n);$$
$$l = 1; 2; \ldots; n \tag{21}$$

where $k_l \in [1;\ p]$, p is the highest order of the defined polynomial. The coefficient $x_{l;k_1k_2\cdots k_{n-1}}(t)$ corresponding to the lth state variable is[40]

$$x_{l;k_1k_2\cdots k_n}(t) = \begin{cases} -/_0(\acute{}_1);\ k_1 = k_2 = \cdots = k_n \\ 1;\ k_1 = 1 \& k_2 = k_3 = \cdots = k_n \\ 0;\ \text{otherwise}\end{cases} \tag{22}$$

$/_0(\acute{}_1)$ denotes the zeroth-order term of the orthogonal polynomial of degree one with $q_{\acute{}_l}(\acute{}_l)$.

Then, the equivalent DDEs expressed using the updated basis are reconstructed as follows

$$\begin{aligned}&\sum_{k_1+k_2\cdots+k_n}\dot{r}_{k_1k_2\cdots k_n}(t)/_{k_1}(\acute{}_1)/_{k_2}(\acute{}_2)\cdots/_{k_n}(\acute{}_n) \\ &= \left(\sum_{k_1+k_2\cdots+k_n} V_{k_1k_2\cdots k_{n-1}}(t)/_{k_1}(\acute{}_1)/_{k_2}(\acute{}_2)\cdots/_{k_n}(\acute{}_n)\right) \\ &\cdot \cos\left(\sum_{k_1+k_2\cdots+k_n} c_{k_1k_2\cdots k_n}(t)/_{k_1}(\acute{}_1)/_{k_2}(\acute{}_2)\cdots/_{k_n}(\acute{}_n)\right)\end{aligned} \tag{23}$$

$$\sum_{k_1+k_2\cdots+k_n} h_{k_1k_2\cdots k_n}(t)/_{k_1}(\varepsilon_1)/_{k_2}(\varepsilon_2)\cdots/_{k_n}(\varepsilon_n) = \left(\sum_{k_1+k_2\cdots+k_n} V_{k_1k_2\cdots k_{n-1}}(t)/_{k_1}(\varepsilon_1)/_{k_2}(\varepsilon_2)\cdots/_{k_n}(\varepsilon_n)\right)\cdot\sin\left(\sum_{k_1+k_2\cdots+k_n} c_{k_1k_2\cdots k_n}(t)/_{k_1}(\varepsilon_1)/_{k_2}(\varepsilon_2)\cdots/_{k_n}(\varepsilon_n)\right) \tag{24}$$

$$\begin{aligned}&\sum_{k_1+k_2\cdots+k_n} V_{k_1k_2\cdots k_n}(t)/_{k_1}(\varepsilon_1)/_{k_2}(\varepsilon_2)\cdots/_{k_n}(\varepsilon_n)\\ &= \frac{\sum_{k_1+k_2\cdots+k_n} T_{k_1k_2\cdots kn}(t)/_{k_1}(\varepsilon_1)/_{k_2}(\varepsilon_2)\cdots/_{k_n}(\varepsilon_n)\cdot\cos\left(\sum_{k_1+k_2\cdots+k_n} a_{k_1k_2\cdots kn}(t)/_{k_1}(\varepsilon_1)/_{k_2}(\varepsilon_2)\cdots/_{k_n}(\varepsilon_n)\right)}{\sum_{k_1+k_2\cdots+k_n} m_{vehiclek_1k_2\cdots k_n}(t)/_{k_1}(\varepsilon_1)/_{k_2}(\varepsilon_2)\cdots/_{k_{n-1}}(\varepsilon_{n-1})}\\ &- \frac{\sum_{k_1+k_2\cdots+k_n} T_{k_1k_2\cdots kn}(t)/_{k_1}(\varepsilon_1)/_{k_2}(\varepsilon_2)\cdots/_{k_n}(\varepsilon_n)}{\sum_{k_1+k_2\cdots+k_n} m_{vehiclek_1k_2\cdots k_n}(t)/_{k_1}(\varepsilon_1)/_{k_2}(\varepsilon_2)\cdots/_{k_{n-1}}(\varepsilon_{n-1})} - \frac{l_g}{r_g^2}\sin\left(\sum_{k_1+k_2\cdots+k_n} c_{k_1k_2\cdots k_n}(t)/_{k_1}(\varepsilon_1)/_{k_2}(\varepsilon_2)\cdots/_{k_n}(\varepsilon_n)\right)\end{aligned} \tag{25}$$

$$\begin{aligned}&\sum_{k_1+k_2\cdots+k_n} c_{k_1k_2\cdots k_n}(t)/_{k_1}(\varepsilon_1)/_{k_2}(\varepsilon_2)\cdots/_{k_n}(\varepsilon_n)\\ &= \frac{\sum_{k_1+k_2\cdots+k_n} T_{k_1k_2\cdots kn}(t)/_{k_1}(\varepsilon_1)/_{k_2}(\varepsilon_2)\cdots/_{k_n}(\varepsilon_n)}{\sum_{k_1+k_2\cdots+k_n} m_{vehiclek_1k_2\cdots kn}(t)/_{k_1}(\varepsilon_1)/_{k_2}(\varepsilon_2)\cdots/_{k_n}(\varepsilon_n)}\frac{\sin\left(\sum_{k_1+k_2\cdots+k_n} a_{k_1k_2\cdots kn}(t)/_{k_1}(\varepsilon_1)/_{k_2}(\varepsilon_2)\cdots/_{k_n}(\varepsilon_n)\right)}{\sum_{k_1+k_2\cdots+k_n} V_{k_1k_2\cdots kn}(t)/_{k_1}(\varepsilon_1)/_{k_2}(\varepsilon_2)\cdots/_{k_n}(\varepsilon_n)}\\ &+ \frac{\sum_{k_1+k_2\cdots+k_n} L_{k_1k_2\cdots kn}(t)/_{k_1}(\varepsilon_1)/_{k_2}(\varepsilon_2)\cdots/_{k_n}(\varepsilon_n)}{\sum_{k_1+k_2\cdots+k_n} m_{vehiclek_1k_2\cdots kn}(t)/_{k_1}(\varepsilon_1)/_{k_2}(\varepsilon_2)\cdots/_{k_n}(\varepsilon_n)\sum_{k_1+k_2\cdots+k_n} V_{k_1k_2\cdots kn}(t)/_{k_1}(\varepsilon_1)/_{k_2}(\varepsilon_2)\cdots/_{k_n}(\varepsilon_n)}\\ &- \frac{l_g}{r_g}\frac{\cos\left(\sum_{k_1+k_2\cdots+k_n} c_{k_1k_2\cdots kn}(t)/_{k_1}(\varepsilon_1)/_{k_2}(\varepsilon_2)\cdots/_{k_n}(\varepsilon_n)\right)}{\sum_{k_1+k_2\cdots+k_n} V_{k_1k_2\cdots kn}(t)/_{k_1}(\varepsilon_1)/_{k_2}(\varepsilon_2)\cdots/_{k_n}(\varepsilon_n)} + \frac{\sum_{k_1+k_2\cdots+k_n} V_{k_1k_2\cdots kn}(t)/_{k_1}(\varepsilon_1)/_{k_2}(\varepsilon_2)\cdots/_{k_n}(\varepsilon_n)}{r_g}\cdot\\ &\qquad\cos\left(\sum_{k_1+k_2\cdots+k_{n-1}} c_{k_1k_2\cdots k_{n-1}}(t)/_{k_1}(\varepsilon_1)/_{k_2}(\varepsilon_2)\cdots/_{k_n}(\varepsilon_n)\right)\end{aligned} \tag{26}$$

$$\sum_{k_1+k_2\cdots+k_n} a_{k_1k_2\cdots k_n}(t)/_{k_1}(\varepsilon_1)/_{k_2}(\varepsilon_2)\cdots/_{k_n}(\varepsilon_n) = \left(\sum_{k_1+k_2\cdots+k_n} q_{k_1k_2\cdots k_n}(t)/_{k_1}(\varepsilon_1)/_{k_2}(\varepsilon_2)\cdots/_{k_n}(\varepsilon_n)\right) - \sum_{k_1+k_2\cdots+k_n} c_{k_1k_2\cdots k_n}(t)/_{k_1}(\varepsilon_1)/_{k_2}(\varepsilon_2)\cdots/_{k_n}(\varepsilon_n) \tag{27}$$

$$\sum_{k_1+k_2\cdots+k_n} q_{k_1k_2\cdots k_n}(t)/_{k_1}(\varepsilon_1)/_{k_2}(\varepsilon_2)\cdots/_{k_{n-1}}(\varepsilon_n) = \frac{\sum_{k_1+k_2\cdots+k_n} M_{k_1k_2\cdots k_n}(t)/_{k_1}(\varepsilon_1)/_{k_2}(\varepsilon_2)\cdots/_{k_{n-1}}(\varepsilon_n)}{I_y} \tag{28}$$

$$\sum_{k_1+k_2\cdots+k_n} m_{vehiclek_1k_2\cdots k_n}(t)/_{k_1}(\varepsilon_1)/_{k_2}(\varepsilon_2)\cdots/_{k_{n-1}}(\varepsilon_n) = -\frac{\sum_{k_1+k_2\cdots+k_n} T_{k_1k_2\cdots k_n}(t)/_{k_1}(\varepsilon_1)/_{k_2}(\varepsilon_2)\cdots/_{k_{n-1}}(\varepsilon_n)}{g_0\sum_{k_1+k_2\cdots+k_n} I_{spk_1k_2\cdots k_n}(t)/_{k_1}(\varepsilon_1)/_{k_2}(\varepsilon_2)\cdots/_{k_{n-1}}(\varepsilon_n)} \tag{29}$$

For L, D, M, T and I_{sp} in Eqs. (23)–(29) are also updated as random variables affected by $\varepsilon_1;\varepsilon_2;\cdots\varepsilon_n$. Because the system state will become random state variable with the integration of Eq. (17), and according to the dynamic models (2)-(3), these aerodynamic forces and moments are related to the system state.

Multiplying both sides of Eqs. (23)–(29) by $/_{k_1}(\varepsilon_1)q_{\varepsilon_1}/_{k_2}(\varepsilon_2)q_{\varepsilon_2}\cdots/_{k_n}(\varepsilon_n)q_{\varepsilon_n}$, and performing n-fold integration on $\varepsilon_1;\varepsilon_2;\cdots\varepsilon_n$ invoke the orthogonality of basis function $/_{k_1}(\varepsilon_1)/_{k_2}(\varepsilon_2)\cdots/_{k_{n-1}}(\varepsilon_n)$. Then, the updated equivalent DDEs of Eqs. (23)–(29) are converted to:

$$x_{\underline{1};k_1k_2\cdots k_n}(t) = \frac{\cdots\int F_{x_l}(\varepsilon_1;\varepsilon_2\ldots;\varepsilon_n;t)/_{k_1}(\varepsilon_1)/_{k_2}(\varepsilon_2)\cdots/_{k_n}(\varepsilon_n)q_{\varepsilon_1\varepsilon_2\ldots\varepsilon_n}d\varepsilon_1d\varepsilon_2\cdots d\varepsilon_n}{\left\langle/_{k_1}(\varepsilon_1)^2\right\rangle\left\langle/_{k_2}(\varepsilon_2)^2\right\rangle\cdots\left\langle/_{k_n}(\varepsilon_n)^2\right\rangle} \tag{30}$$

where $F_{x_l}(\varepsilon_1;\varepsilon_2\ldots;\varepsilon_n;t)$ represents the expression on the right side of Eqs. (23)-(29). $q_{\varepsilon_1\varepsilon_2\ldots\varepsilon_n}$ is the joint PDF of $\varepsilon_1;\varepsilon_2\ldots;\varepsilon_n$, and since $\varepsilon_1;\varepsilon_2\ldots;\varepsilon_n$ are statistically independent, $q_{\varepsilon_1\varepsilon_2\ldots\varepsilon_n} = q_{\varepsilon_1}q_{\varepsilon_2}\cdots q_{\varepsilon_n}$.

In practice, to reduce the computational burden of multiple integrals and joint PDF $q_{\varepsilon_1\varepsilon_2\ldots\varepsilon_n}$ in Eq. (30), an integral conversion is usually required. According to Ref. 41, the relationship between $q_{\varepsilon_1\varepsilon_2\ldots\varepsilon_n}$ and $q(D)$ is

$$\cdots\int q_{\varepsilon_1\varepsilon_2\ldots\varepsilon_n}d\varepsilon_1d\varepsilon_2\cdots d\varepsilon_n = \int q(D)dD \tag{31}$$

Then, the n-fold integral and joint PDF in Eq. (30) can be transformed into

$$\begin{aligned}&\cdots\int F_{x_l}(\varepsilon_1;\varepsilon_2\ldots;\varepsilon_n;t)q_{\varepsilon_1\varepsilon_2\ldots\varepsilon_n}d\varepsilon_1d\varepsilon_2\cdots d\varepsilon_n\\ &= \int F(Z_1(D);Z_2(D);\cdots;Z_n(D))q(D)dD\end{aligned} \tag{32}$$

Based on Eq. (19), $/_{k_l}(\varepsilon_l)$ can be obtained by

$$/_{k_l}(\varepsilon_l) = /_{k_l}(Z_l(D));\ l = 1;2;\ldots;n \tag{33}$$

Consequently, Eq. (30) can be transformed into the following updated equivalent DDEs:

$$x_{\underline{1};k_1k_2\cdots k_n}(t) = \frac{\int F(Z_1(D);Z_2(D);\cdots;Z_n(D))/_{k_1}(Z_1(D))/_{k_2}(Z_2(D))\cdots/_{k_n}(Z_n(D))q(D)dD}{\left\langle/_{k_1}(Z_1(D))^2\right\rangle\left\langle/_{k_2}(Z_2(D))^2\right\rangle\cdots\left\langle/_{k_n}(Z_n(D))^2\right\rangle} \tag{34}$$

where $k_1k_2\cdots k_n = 0;1;\ldots;N_p$, $l = 1;2;\ldots;n$.

Furthermore, the variation of state space of stochastic system needs to be considered. Although the initial state is determined when $t = t_0$, under the integral effect, the system state at the next moment is uncertain due to the uncertainty of state differential equations. Hence, the adaptive polynomial chaos algorithm also need to update the parameters of stochastic system state. The update criterion is [42]:

$$\left(\frac{1}{r_{l;p}^2}\sum_{k_1+k_2\cdots+k_n=N_{p-1}+1}^{N_p}\hat{x}_{l;k_1k_2\cdots k_n}^2\left\langle \xi_{k_1}(\xi_1)^2\right\rangle\left\langle \xi_{k_2}(\xi_2)^2\right\rangle\cdots\left\langle \xi_{k_n}(\xi_n)^2\right\rangle\right)^{v}\Pr(I_k=1)$$
$$P \geq \eta_1 \tag{35}$$

where

$$I_k=\begin{cases}1; & \text{if } \xi\in B_k\\ 0; & \text{otherwise}\end{cases}$$
$$\Pr(I_k=1):=\prod_{i=1}^{n}\frac{b_i-a_i}{2};\quad r_{l;p}^2=\sum_{k_1+k_2\cdots+k_n=1}^{N_p}\hat{x}_{l;k_1k_2\cdots k_n}^2\left\langle \xi_{k_1}(\xi_1)^2\right\rangle\left\langle \xi_{k_2}(\xi_2)^2\right\rangle\cdots\left\langle \xi_{k_n}(\xi_n)^2\right\rangle \tag{36}$$

where $\xi=[\xi_1;\xi_2;\ldots;\xi_n]$, $\eta_{k_j}(\xi_j)$ is the updated orthogonal basis, and $\hat{x}_{l;k_1k_2\cdots k_n}$ is the polynomial chaos coefficients of lth stochastic state at the previous time. The threshold parameters $v\in(0;\ 1)$, $\eta_1\in(0;\ 0.1]$. $B_k=[a_1;\ b_1)\times\cdots\times(a_n;b_n]$, a_l and b_l are the upper and lower bounds of the random space of lth state, respectively. If the condition (35) is satisfied, the subsequent operation will be performed to decompose the random space to update the stochastic state parameters.

The state parameter $\hat{x}_l$ at the previous moment is expressed by the new orthogonal basis as

$$\hat{x}_l(D)=\sum_{i=0}\hat{x}_{li}\eta_i(\xi) \tag{37}$$

The expression of random field of update status can be written as follows:

$$\tilde{x}_l(\xi)=\sum_{i=0}\tilde{x}_{li}\eta_i(\xi) \tag{38}$$

where $\xi\in[-1;1]^n$, and the mapping relationship between D and ξ is $\xi=Z(D)$, $Z=\mathrm{diag}[Z_1;Z_2;\ldots;Z_n]$, the expression of Z_l is shown in Eq. (19). To determine the coefficient $\tilde{x}_{li}$, N_p+1 uniform grid points ξ_j are selected in $[-1;1]^n$, and the random space $[-1;1]$ of ξ_j is decomposed into two equal dimensional spaces $[-1;0]$ and $[0;1]$. Based on these discrete grid points, the following state-space equation can be obtained

$$\begin{bmatrix}u_{00} & u_{10} & \cdots & u_{N_p0}\\ u_{01} & u_{11} & \cdots & u_{N_p1}\\ \vdots & \vdots & \vdots & \vdots\\ u_{0N_p} & u_{1N_p} & \cdots & u_{N_pN_p}\end{bmatrix}\begin{bmatrix}\tilde{x}_{l0}\\ \tilde{x}_{l1}\\ \vdots\\ \tilde{x}_{lN_p}\end{bmatrix}=\begin{bmatrix}\sum_{i=0}^{N_p}\hat{x}_{li}\eta_i(Z^{-1}(\xi_0))\\ \sum_{i=0}^{N_p}\hat{x}_{li}\eta_i(Z^{-1}(\xi_1))\\ \vdots\\ \sum_{i=0}^{N_p}\hat{x}_{li}\eta_i(Z^{-1}(\xi_{N_p}))\end{bmatrix} \tag{39}$$

where $\eta_{ij}=\eta_i(\xi_j)$, $j\in[0;N_p]$. For ease of description, Eq. (39) can be rewritten to

$$A_\eta\tilde{x}_l=\hat{x}_l \tag{40}$$

since A_η is composed of orthogonal basis, A_η^{-1} exists for any ξ_i in $[-1;1]^n$. Then, $\tilde{x}_l$ can be solved as

$$\tilde{x}_l=A_\eta^{-1}\hat{x}_l \tag{41}$$

thus, the initial state space of stochastic system at the next moment is updated.

Then, the new DDEs should be employed until a next time level t_2, at which criterion (18) is fulfilled again. Next, Eq. (20) is used to update the PDF of random variable, and apply the Schmidt orthogonalization rule to obtain the corresponding orthogonal basis. At the same time, judge whether Eq. (35) is true. If so, use Eq. (39) and Eq. (41) to update the initial state space of stochastic system. Finally, the updated DDEs are obtained by Eq. (34). The process should be repeated until the end of the integration. The adaptive polynomial chaos algorithm can be summarized as:

Algorithm 1. Adaptive polynomial chaos algorithm

Step 1.	If the indicator (18) satisfies, enter to Step 2, otherwise, perform the following steps. • The updated random variable ξ_{new} is obtained via Eq. (19). • Calculate the PDF of ξ_{new} by Eq. (20). • Gram–Schmidt orthogonalization: create a random trial basis $\{\eta_i(\xi_{new})\}$
Step 2.	If the Eq. (35) holds, enter to Step 3; otherwise, Eq. (39) and Eq. (41) are used to update the initial state space of the equivalent DDEs.
Step 3.	Update DDEs via Eq. (34).

Under the condition of uncertain aerodynamic coefficient, the extended state constraints of (4c) and (11) determined by PCE are as follows:

$$a_{min}\leq a_0(t)-r(a(t));\ a_0(t)+r(a(t))\leq G_a(Ma) \tag{42}$$

$$\begin{cases}\max\{|V_{f;0}+r(V_f)-V_T|;|V_{f;0}-r(V_f)-V_T|\}\leq dV_{f;max}\\ \max\{|h_{f;0}+r(h_f)-h_T|;|h_{f;0}-r(h_f)-h_T|\}\leq dh_{f;max}\\ \max\{|r_{f;0}+r(r_f)-r_T|;|r_{f;0}-r(r_f)-r_T|\}\leq dr_{f;max}\end{cases} \tag{43}$$

where

$$r(a(t))=\sqrt{a_1(t)^2+a_2(t)^2+\cdots+a_{N_p}(t)^2};\ r(V_f)=\sqrt{V_{f;1}^2+V_{f;2}^2+\cdots+V_{f;N_p}^2}$$
$$r(h_f)=\sqrt{h_{f;1}^1+h_{f;2}^2+\cdots+h_{f;N_p}^2};\ r(r_f)=\sqrt{r_{f;1}^2+r_{f;2}^2+\cdots+r_{f;N_p}^2}$$

$r(\cdot)$ represents standard deviation. a_i, V_i, h_i, and r_i $(i=0;1;\ldots;N_p)$ are the i + 1th PCE coefficients of angle of attack, velocity, height and horizontal displacement respectively, which are obtained by integrating the above DDEs. Ref. 37 indicates that the first PCE coefficient of a random variable represents its average value.

3.2. Optimal control command design for uncertain system

For an uncertain system, in order to obtain the robust control command u^*, the cost function of deterministic optimization problem must be modified. For uncertain system control optimization, the information (mean $E(\cdot)$ and variance $r^2(\cdot)$) of stochastic state needs to be taken into account in the cost function. This information can be described by the state of augmented system, which is generated by the PCE method described in Section 3.1.

Then, the Augmented Optimal Control Problem (AOCP) considering system uncertainty can be described by the following equation

$$\begin{aligned} \min\ & J_{AOCP} = g_1 J_0 + g_2\left(U[E(X); r^2(X)] + \int_{t_0}^{t_f} W[E(X); r^2(X)]dt\right) \\ & \text{s.t:} \quad \text{Eqs:}(34);(4a)-(4b);(42);(43) \end{aligned} \tag{44}$$

where J_0 represents the performance index (10) of deterministic OCP, $U\left[E\left[X^2\right]; r^2(X)\right]$ indicates the terminal optimization form, the purpose is to minimize the statistical information of random variable at the terminal of trajectory. $\int_{t_0}^{t_f} W\left[E\left[X^2\right]; r^2(X)\right]dt$ expresses the integral optimization form, to minimize the mean or variance of random variables throughout the flight segment. g_1 and g_2 are the weight values of J_0 and statistical information, respectively.

From Ref. 14 and Ref. 37, we can know that the average of uncertain parameter is the first value of its corresponding PCE coefficient, and its variance is the sum of squares of the corresponding PCE coefficients except for the first coefficient. Therefore, the mean and variance information of uncertain system can be expressed by Eqs. (45)–(46), and written into the cost function.

$$E(X) = X(t)^T F$$

$$F = \begin{bmatrix} 1 & 0 & \cdots & 0 & 0 & \cdots & 0 & 0 & \cdots & 0 \\ 0 & 0 & \cdots & 0 & 0 & \cdots & 0 & 0 & \cdots & 0 \\ 0 & 0 & \cdots & 0 & 0 & \cdots & 0 & 0 & \cdots & 0 \\ \vdots & \vdots & \cdots & \vdots & \vdots & \cdots & \vdots & \vdots & \cdots & \vdots \\ 0 & 0 & \cdots & 1_{(N_p+2;N_p+2)} & 0 & \cdots & 0 & 0 & \cdots & 0 \\ 0 & 0 & \cdots & 0 & 0 & \cdots & 0 & 0 & \cdots & 0 \\ \vdots & \vdots & \cdots & \vdots & \vdots & \ddots & \vdots & \vdots & \cdots & \vdots \\ 0 & 0 & \cdots & 0 & 0 & \cdots & 1_{((N_p+1)\cdot(n-1)+1;(N_p+1)\cdot(n-1)+1)} & 0 & \cdots & 0 \\ 0 & 0 & \cdots & 0 & 0 & \cdots & 0 & 0 & \cdots & 0 \\ 0 & 0 & \cdots & 0 & 0 & \cdots & 0 & 0 & \cdots & 0 \end{bmatrix}_{n(N_p+1)\times n(N_p+1)} \tag{45}$$

$$r^2(X) = S_{diag}\left(H(X)H(X)^T\right) - E[X]^2$$

$$H(X) = \begin{bmatrix} X_1 & X_2 & \cdots & X_{N_p+1} & 0 & 0 & \cdots & 0 & 0 & \cdots & 0 & 0 & \cdots & 0 \\ 0 & 0 & 0 & 0 & X_{N_p+2} & X_{N_p+3} & \cdots & X_{2(N_p+1)} & 0 & \cdots & 0 & 0 & \cdots & 0 \\ \vdots & \vdots & \vdots & \vdots & \vdots & \vdots & \cdots & \vdots & \vdots & \cdots & \vdots & \vdots & \cdots & \vdots \\ 0 & 0 & 0 & 0 & 0 & 0 & \cdots & 0 & 0 & \cdots & X_{(n-1)\cdot(N_p+1)+1} & X_{(n-1)\cdot(N_p+1)+2} & \cdots & X_{n\cdot(N_p+1)} \end{bmatrix}_{n\times n(N_p+1)} \tag{46}$$

where $X \in R^{n(N_p+1)}$ represents the state variable of the augmented matrix, $S_{diag}(\cdot)$ is the function of extracting diagonal elements of matrix $H(X)H(X)^T$.

Then, the optimization problem (44) is solved to obtain the robust optimization control commands of uncertain system. The proposed Robust Control Command Optimization (RCCO) method can be summarized into the following steps, and the implementation process is shown in Fig. 5.

Algorithm 2. Robust control command optimization method based on PCE

Step 1.	Parameters of PIO algorithm: initial pigeon population size N_{pop}, design variable $u_{design} = [t; d_e(t); /_F(t)]$ ($t = \{t_1; t_2; \ldots; t_i; \ldots; t_{N_t}\}$ is the discrete time), PIO operator and maximum number of iterations k_{max}. Let $k_i = 1$.
Step 2.	Randomly generate N_{pop} group design variables u_{design} satisfying constraints (4a) and (4b).

Algorithm 2. (continued)

Algorithm 2. Robust control command optimization method based on PCE	
Step 3.	Based on the parameter u_{design}, the initial state value and the set random input, the equivalent DDEs of RDEs are constructed by PCE. The terminal time given by u_{design} is denoted as t_f, $t_f = t_{N_t}$.
Step 4.	The discrete time of sampling is $\{t_1; t_2; \ldots; t_i; \ldots; t_{N_t}\}$, and let $i = 1$.
Step 5.	Integrate DDEs over time $[t_{i-1}; t_i]$.
Step 6.	Update the DDEs at t_i time via Algorithm 1.
Step 7.	If $i < N_t$, let $i = i + 1$ and return to Step 5, otherwise, output the state X of augmented system.
Step 8.	Repeat Step 3-Step 7 until states $\{X^1; X^2; \ldots; X^{N_{pop}}\}$ of N_{pop}-group augmented system are obtained. Then, $\{X^1; X^2; \ldots; X^{N_{pop}}\}$ are substituted into Eq. (44) to obtain the optimal parameter u^* satisfying the constraints (42)–(43).
Step 9.	Update the design variable by the PIO operator, denoted as u_{new}. Execute Step 3-Step 7 to obtain X^{new}. Then, the X^{new} and the X^* corresponding to u^* are substituted into Eq. (44). If $J_{AOCP}(u_{new}) < J_{AOCP}(u^*)$, u^* is updated to $u^* = u_{new}$; otherwise, continue to Step 10.
Step 10.	If $k_i > k_{max}$, go to Step 11; otherwise, let $k_i = k_i + 1$, and return to Step 9.
Step 11.	Whether the statistical information $J_s = U[E(x); r^2(x)] + \int_{t_0}^{t_f} W[E(x); r^2(x)]dt$ of random variable in the cost function is less than the set value d_{max} (d_{max} is set manually). If it is satisfied, the robust optimal control command u^* is obtained; otherwise, the weight value g_2 is adjusted, let $k_i = 1$, and return to Step 9.

4. Analysis and application

In this section, first analyze the effectiveness of augmented system generated via the PCE method in predicting the evolution of uncertain systems. Then, a robust ascent trajectory of GHAME is designed by the RCCO method. Finally, the optimization results of the RCCO method and the deterministic optimization method PIO[9] are applied to the GHAME vehicle respectively, and the results are compared to verify the effectiveness of present algorithm.

4.1. Perturbation analysis of aerodynamic parameters

Taking the motion characteristics analysis of GHAME model[33] with parameter uncertainties as an example, the effectiveness of the above-mentioned method for describing the uncertain system is verified. The short-period approximate model of the GHAME vehicle in the trimming condition of 3 Ma, 15 km is taken as an example. For simplicity, it is assumed that the system parameters are dependent on a single random variable D. The short-period state vector is $X_{short} = [a; q; g_e]^T$, g_e is the measured elevator state. The control input $u = d_e$ is the elevator command (the unit is degree). The matrix values in the vehicle model are as follows:

$$\begin{cases} A = \begin{bmatrix} -0{:}6398 & 0{:}9378 & -0{:}0014 \\ -1{:}5679(1+D) & -0{:}8791(1+D) & -0{:}1137(1+D) \\ 0 & 0 & -20{:}2 \end{bmatrix} \\ B = [0; 0; 20{:}2]^T \\ C = \left[0; \frac{180}{p}; 0\right] \end{cases} \tag{47}$$

Assume that the probability distribution of random variable D is the uniform distribution, and $D \in [-0{:}2; 0{:}2]$. Set the highest order of orthogonal basis $p = 4$, and the necessary parameters for the criteria are $\mathbb{m}_1 = \mathbb{m}_2 = \mathbb{m}_3 = 2\text{=}3$, $v = 0{:}5$, and $\#_1 = 10^{-2}$, respectively. The augmented matrix after uncertainty quantification is represented by $\tilde{A}$, as shown below:

$$\tilde{A} = \begin{bmatrix}
-0{:}6398 & 0 & 0 & 0 & 0 & 0{:}9378 & 0 & 0 & 0 & 0 & -0{:}0014 & 0 & 0 & & \\
0 & -0{:}6398 & 0 & 0 & 0 & 0 & 0{:}9378 & 0 & 0 & 0 & 0 & -0{:}0014 & 0 & & \\
0 & 0 & -0{:}6398 & 0 & 0 & 0 & 0 & 0{:}9378 & 0 & 0 & 0 & 0 & -0{:}0014 & & \\
0 & 0 & 0 & -0{:}6398 & 0 & 0 & 0 & 0 & 0{:}9378 & 0 & 0 & 0 & 0 & -0{:}0014 & \\
0 & 0 & 0 & 0 & -0{:}6398 & 0 & 0 & 0 & 0 & 0{:}9378 & 0 & 0 & 0 & 0 & -0{:}0014 \\
-1{:}5679 & -0{:}1045 & 0 & 0 & 0 & -0{:}8791 & -0{:}0586 & 0 & 0 & 0 & -0{:}1137 & -0{:}0076 & 0 & 0 & 0 \\
-0{:}3136 & -1{:}5679 & -0{:}1254 & 0 & 0 & -0{:}1758 & -0{:}8791 & -0{:}0703 & 0 & 0 & -0{:}0227 & -0{:}1137 & -0{:}0091 & 0 & 0 \\
0 & -0{:}2091 & -1{:}5679 & -0{:}1344 & 0 & 0 & -0{:}1172 & -0{:}8791 & -0{:}0754 & 0 & 0 & -0{:}0152 & -0{:}1137 & -0{:}0097 & 0 \\
0 & 0 & -0{:}1881 & -1{:}5679 & -0{:}1394 & 0 & 0 & -0{:}1055 & -0{:}8791 & -0{:}0781 & 0 & 0 & -0{:}0136 & -0{:}1137 & -0{:}0101 \\
0 & 0 & 0 & -0{:}1792 & -1{:}5679 & 0 & 0 & 0 & -0{:}1005 & -0{:}8791 & 0 & 0 & 0 & -0{:}0130 & -0{:}1137 \\
0 & 0 & 0 & 0 & 0 & 0 & 0 & 0 & 0 & 0 & -20{:}2 & 0 & 0 & 0 & 0 \\
0 & 0 & 0 & 0 & 0 & 0 & 0 & 0 & 0 & 0 & 0 & -20{:}2 & 0 & 0 & 0 \\
0 & 0 & 0 & 0 & 0 & 0 & 0 & 0 & 0 & 0 & 0 & 0 & -20{:}2 & 0 & 0 \\
0 & 0 & 0 & 0 & 0 & 0 & 0 & 0 & 0 & 0 & 0 & 0 & 0 & -20{:}2 & 0 \\
0 & 0 & 0 & 0 & 0 & 0 & 0 & 0 & 0 & 0 & 0 & 0 & 0 & 0 & -20{:}2
\end{bmatrix}$$

Figs. 6-7 show the prediction ability of augmented system to the dynamic characteristics of uncertain system (47). In

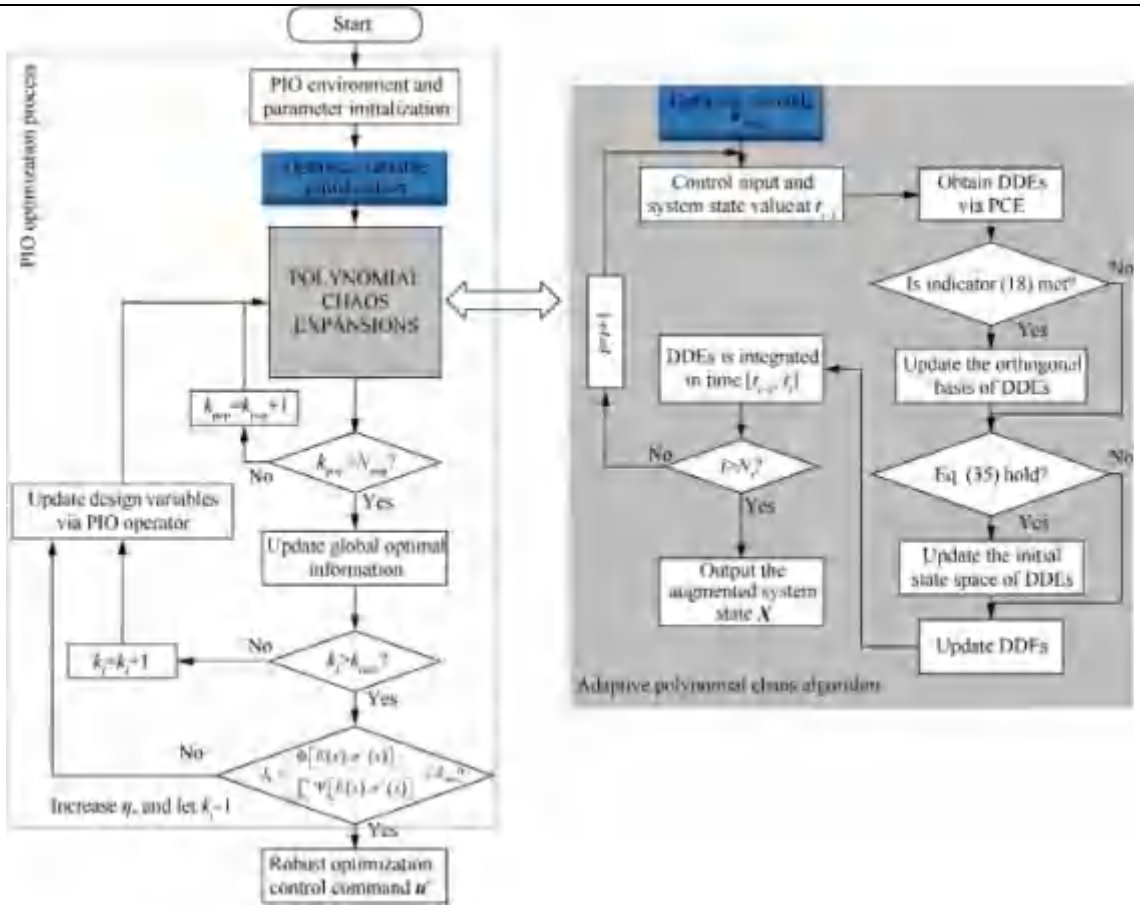

Fig. 5 Robust control command optimization strategy based on polynomial chaos.

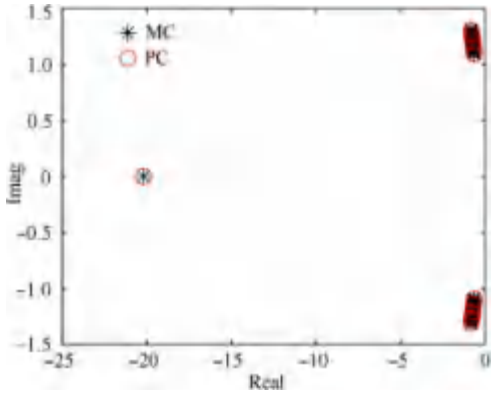

Fig. 6 Closed loop eigenvalue distributions for a short-period mode for ±20% parameter uncertainty.

Fig. 6, the circles represent the eigenvalues of augmented system, and ∗ represents the eigenvalues of uncertain system obtained by MC simulation. Fig. 7 shows the pitch rate response of the system with 20% uncertainty in the aforementioned parameters. The predicted trajectory bounds obtained by PCE, and pitch rate curves given via MC are represented by dashed-lines and dark-solid lines, respectively.

According to Fig. 6, the augmented system can capture the eigenvalue distribution of uncertain system. In addition, it can

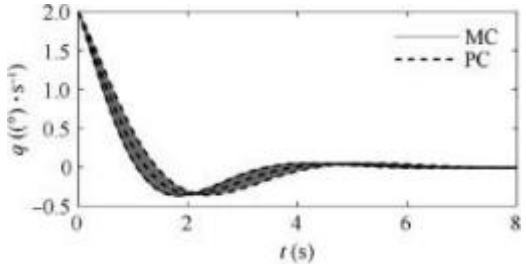

Fig. 7 PC and MC system response to ±20% parameter uncertainty.

be seen from Fig. 7 that the bounds predicted by the augmented system are in excellent agreement with the pitch rate curves obtained by the MC method. The simulation results show that the augmented system generated by the improved PCE algorithm can be applied to predict the kinematic characteristics of uncertain system and analyze its stability, which has higher computational efficiency than the MC method.

4.2. Robust optimization design of control command

4.2.1. Simulation conditions

In this section, the proposed method is applied to the GHAME vehicle, and the effectiveness of method is verified

by simulation. Set the initial state as: $Ma(t_0) = 5$, $h(t_0) = 20{:}4$ km, $r(t_0) = 0$ km, $a(t_0) = 2^o$, $c(t_0) = 10^o$, $m_{vehicle}(t_0) = 116077$ kg; The ascent target point is: $Ma_T = 10$, $h_T = 34{:}6$ km, $r_T = 79{:}7$ km. Define the aerodynamic force Coefficient of Coincidence (COC) K_A to describe the aerodynamic perturbation during the ascent, the lift and drag can be expressed as:

$$L = K_A \frac{C_L q V^2 S_{ref}}{2m_{vehicle}}; \quad D = K_A \frac{C_D q V^2 S_{ref}}{2m_{vehicle}} \tag{48}$$

The $K_A = 1$ means that the actual aerodynamic force is consistent with the nominal aerodynamic force. In actual flight, due to the influence of air density, atmospheric temperature, and airplane structural factors, the COC often varies within a certain range. Therefore, the case of 20% aerodynamic force perturbation is considered, i.e., assumes that $K_A \in [0{:}8;\ 1{:}2]$ and satisfies a uniform distribution.

Compared with the complex constraints faced by ASVs, the simplified version of (4) is considered in the simulation, as shown below:

$$\begin{gathered} -15^o \leq d_e \leq 15^o; \quad 0{:}4 \leq /_F \leq 1{:}3 \\ -3^o \leq a \leq G_a(t); \quad G_a(t) \approx G_0 + G_1(Ma_d(t) + n_{Ma}(t)) \end{gathered} \tag{49}$$

where $G_0 = -8$, $G_1 = 2$.[43] Ma_d is the desired Mach number, n_{Ma} is the speed deviation, $Ma_d \gg |n_{Ma}|$. According to the aerodynamic database of GHAME,[33] the minimum negative angle of attack is -3^o, that is, the lower bound of the angle of attack of the GHAME vehicle is -3^o. Then, the final constraint range of AOA is the red shaded part in Fig. 8.

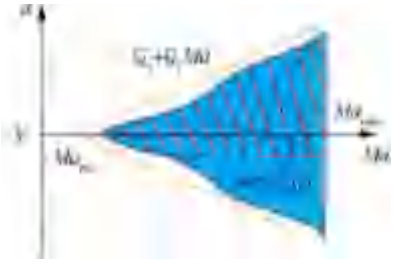

Fig. 8 Angle of attack constraint.

4.2.2. Robust optimization of ascent trajectory

The RCCO method not only considers the system uncertainty in the solution process, but also improves the traditional optimization problem by taking SDF as one of the performance indexes. To verify the effectiveness of proposed method, the ascent trajectory will be designed based on the RCCO method and the traditional optimization method, respectively.

For traditional trajectory optimization, which is designed only for standard systems without the uncertainty, as shown in Eq. (50). The objective function is to minimize fuel consumption and reach the target point. Next, a PIO algorithm in Ref. 9 is used to solve the optimization problem (50).

$$\begin{aligned} \min \ J &= \left\{ d_{mass} + (\| r_f - r_T \|_2 + \| h_f - h_T \|_2) \right\} \\ \text{s:t:} \ & \ \text{Eqs:}(1); (11); (49) \end{aligned} \tag{50}$$

The RCCO method takes into account the uncertainties in the trajectory optimization problem and the solution process. In addition, the SDF of GAHME along the trajectory is considered in the optimization objective function, then the optimization problem (50) is converted to (51).

$$\begin{aligned} \min \ J = g_1(j_1 d_{mass} + j_2(\| r_f - r_T \|_2 + \| h_f - h_T \|_2) + j_3 J_{SDF}) \\ + g_2(r^2(h_f) + r^2(r_f)) \\ \text{s:t:} \ \text{Eqs:}(34); (42); (43); (49) \\ (r^2(h_f) + r^2(r_f)) \leq d_{max} \end{aligned} \tag{51}$$

where $r^2(h_f) + r^2(r_f)$ is the sum of the first two items of $r^2(X)$ calculated by Eq. (46), namely $r^2(h_f) + r^2(r_f) = \underbrace{[1;\ 1;\ 0;\ \cdots;\ 0]}_{n} \cdot r^2(X)$, and set $d_{max} = 5 \times 10^3$. This article chooses $j_1 = 1$, $j_2 = 1$, $j_3 = 1000$, and $g_1 = 1$, $g_2 = 1000$. The highest order of orthogonal basis $p = 4$, and the necessary parameters for the criteria are $\mathbb{m}_l = 1{=}3;\ l = 1; 2; \ldots; n$, $v = 0{:}5$, and $\#_1 = 10^{-2}$, respectively. In the simulation, let $dV_{f;max} = 300$m=s, $dh_{f;max} = 300$ m, $dr_{f;max} = 1000$ m in Eq. (11) and Eq. (43).

Finally, the optimization problems (50) and (51) are solved by PIO method and RCCO method respectively, and the generated optimization control instructions are shown in Fig. 9. In

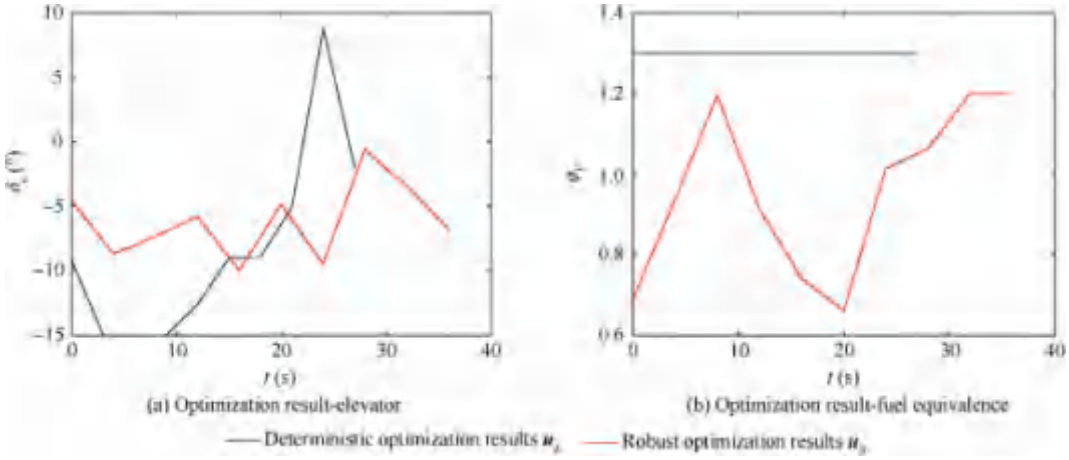

Fig. 9 Optimal control variables obtained by RCCO method and deterministic trajectory optimization method.

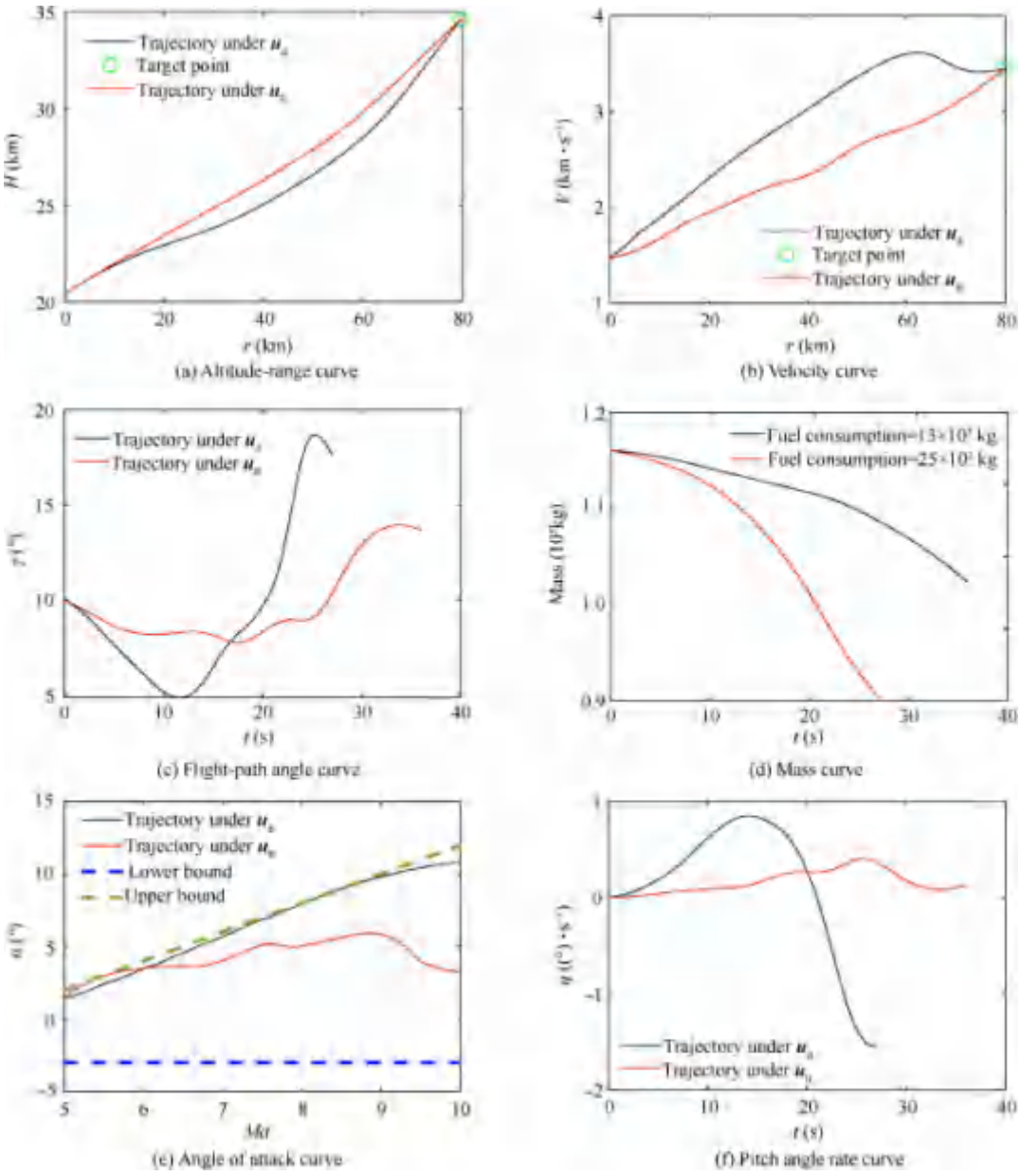

Fig. 10 State variable curves of two systems.

the figure, the black-solid represents the optimal control variable u_d obtained by PIO solving problem (50), and the red-solid represents the optimal control variable u_R given via the RCCO method solving problem (51).

Firstly, the effectiveness of the above two methods for solving optimization problems (50) and (51) is analyzed. The resulted optimization variable u_d is substituted into the deterministic system (1), and u_R is applied into the DDEs constructed in Section 3.1, and the corresponding state variables x_{det} and X_{DDEs} are obtained by integration respectively. In Fig. 10, black-solid lines are the corresponding state curves x_{det} (deterministic system). The red-solid lines are the $E(X_{DDEs})$ curves, which represent the mean values of state variables of the stochastic system (14). The expression of $E(X_{DDEs})$ is Eq. (45). Among them, Fig. 10(e) shows the variation curve of AOA with the Mach number, and the upper and lower boundaries of its constraint at different flight speeds.

According to Fig. 10, the optimization problems (50) and (51) have obtained solutions satisfying state constraints under the corresponding algorithms. In addition, compared with the PIO method, the optimized trajectory via the RCCO method is more gentle. That is, the amplitude and variation rate of state (such as AOA a and fight-path angle c) and the amplitude of control variables (d_e and $/_F$) are smaller. Of course, this also leads to the trajectory optimized by the RCCO method has longer climbing time and greater fuel consumption.

Then, in order to verify the robustness of the optimal control commands obtained by the RCCO method, the u_d and u_R are substituted into the stochastic system (14) for MC simulation. Consider that the aerodynamic parameters of GHAME satisfy Eq. (48), u_d and u_R are respectively applied to this stochastic system for 500 MC simulations. Fig. 11 and Fig. 12 show the MC simulation results of the height-range curve and the velocity-range curve.

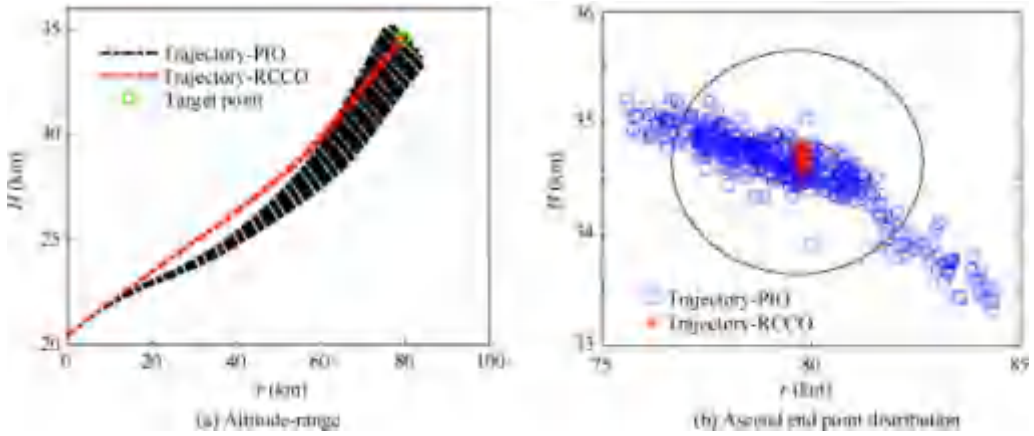

Fig. 11 MC simulation results of altitude-range with aerodynamic parameter uncertainty.

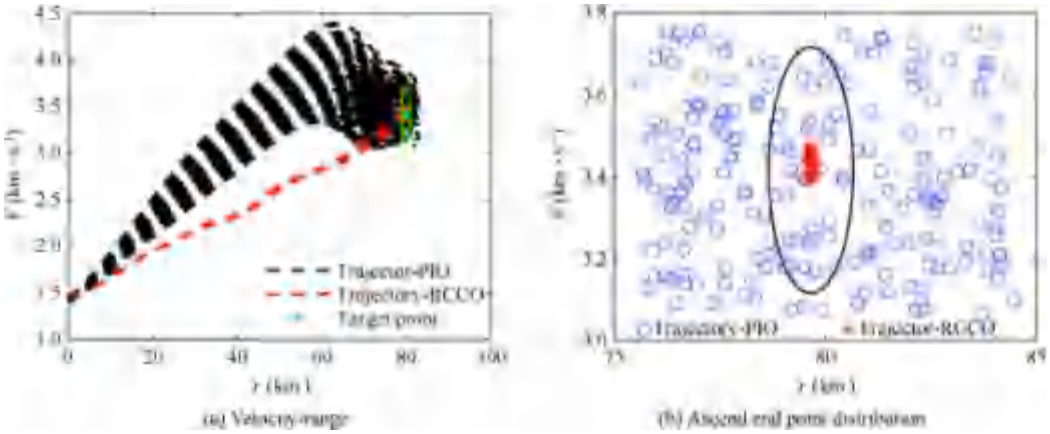

Fig. 12 MC simulation results of velocity-range with aerodynamic parameter uncertainty.

The two ellipses in Fig. 11(b) represent the boundaries corresponding to single and triple of the allowable maximum errors between the terminal position and target position ($dh_{f;max} = 300$ m, $dr_{f;max} = 1000$ m), respectively. The short-axis and long-axis of the first ellipse in Fig. 11(b) represent the distance of 300 m and 1000 m from the height and horizontal displacement of the target point, respectively. And the short-axis and long-axis of the second ellipse are 1000 m and 3000 m. It can be clearly seen from Fig. 11 that the trajectories generated by executing 500 MC under u_R satisfy the set terminal position constraint conditions, and their distribution is relatively concentrated. This indicates that the optimized trajectory given via the RCCO method has strong robustness and terminal position constraint satisfaction ability.

The ellipses in Fig. 12 represent the same implication, which represent the boundary formed by the set terminal velocity and horizontal displacement constraints ($dV_{f;max} = 300$ m=s, $dr_{f;max} = 1000$ m). If the terminal state of trajectory is outside the ellipse, it means that the resulted trajectory does not meet the set terminal constraint. The short and long axes of the ellipse in Fig. 12 are 300 m/s and 1000 m, respectively. According to Fig. 12(a), we can conclude that under the reference control command obtained by the proposed method, the flight speed of GHAME is little affected by the uncertain parameters.

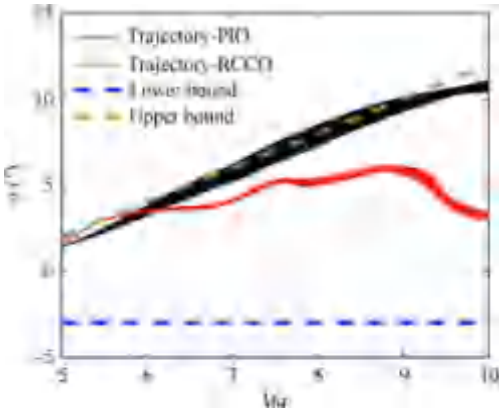

Fig. 13 MC simulation results of AOA and its constraints.

According to Fig. 12(b), it can be seen that under u_R, the variation range of terminal velocity is within the constraint range of the optimization problem (51). However, in the uncertain system, the deterministic optimization results u_d cannot ensure the dispersion degree of terminal velocity and position.

Next, the ability of the RCCO method to satisfy the system state constraints under parameter uncertainties is verified.

Although the AOA shown in Fig. 10 satisfies the constraint (49), it is impossible to prove whether AOA can still meet this constraint within the variation range of all uncertain parameters. Fig. 13 demonstrates these curves of AOA obtained by 500 MC simulations and the constraint of AOA in the ascent phase.

Fig. 13 exhibits that under the uncertain aerodynamic parameters, the reference control commands obtained by the RCCO method can ensure the vehicle still satisfies the constraint of AOA.

According to the above simulation analysis, under the condition of parameter perturbation, the optimization results generated by the traditional deterministic optimization method are larger affected by uncertainty, and would have a large deviation from the nominal trajectory. Thus, it is difficult to adapt to the actual flight environment. In the RCCO method, the influence of uncertainty on the optimization results is fully considered, so the optimization results have excellent robust stability. Moreover, the design variable of RCCO method is the actual control inputs, which can ensure the feasibility of designed trajectory and reduce the burden of control system in dealing with uncertainties.

Finally, the SDF characteristics of GHAME under the ascent trajectory obtained via the RCCO method are evaluated to verify whether the method can optimize the SDF characteristics while ensuring robustness. Fig. 14 describes the short-period flight quality $n_{sp} - x_{sp}^2=(n_z=a)$ of GHAME under the ascent trajectories shown in Fig. 11, where n_z represents the normal overload. In the figure, the green curve is the SDF characteristic trend of GHAME under the trajectory given via the RCCO method, and the orange curve represents the SDF characteristic trend under the trajectory provided by the PIO method.

According to the evaluation results of SDF under different ascent trajectories shown in Fig. 14, along the ascent trajectory obtained by the RCCO method, the SDF characteristics level of GHAME is gradually approaching Level-One. However,

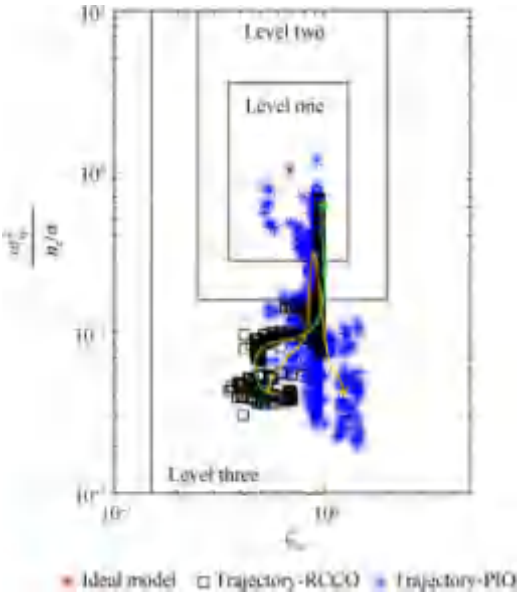

Fig. 14 Flying quality evaluation curve under different ascent trajectories.

under the trajectory generated by solving the optimization problem (50), although the SDF characteristic level has an improvement trend, it finally drops back to Level-Three. It can be concluded that the RCCO method can obtain an ascent trajectory with better flight quality and robustness than the traditional optimization method. Thereby, a good front-end input could be provided to the controller to balance the burden of trajectory planning and control system design.

Based on the above simulation results, it can be seen that the resulted trajectory of the RCCO method is low sensitivity to uncertainty, and the RCCO method can optimize the SDF characteristic while ensuring robustness. However, it consumes 12×10^3kg more fuel than the conventional optimization method. This is also at the expense of fuel consumption to obtain an ascent trajectory with better robustness and control performance.

5. Conclusions

This paper proposes a multi-constraint robust trajectory optimization method. The robust optimization method combines the characteristics of ASVs, improves the traditional deterministic trajectory optimization problem, and takes some control performance as one of the optimization objectives. In addition, this method considers the influence of parameter uncertainty in trajectory optimization. Meanwhile, the actuator saturation constraint, FER constraint, and engine un-start constraint are considered. The proposed method is applied to optimize the ascent trajectory of GHAME with parameter uncertainty to reduce the influence of parameter uncertainty on the designed trajectory.

This robust optimization method takes the actual control input (elevator and FER) as the design variable, which not only ensures that the optimized trajectory is actually controllable, but also enables the SDF characteristic to be considered in the optimization objective. Thus, a reference control command with strong robustness and good SDF characteristic is provided, which reduces the burden of control system. The MC simulation results show that, compared with the traditional deterministic optimization method, the results obtained by the proposed optimization method have better robustness, SDF characteristic, and the ability to satisfy constraints.

Declaration of Competing Interest

The authors declare that they have no known competing financial interests or personal relationships that could have appeared to influence the work reported in this paper.

Acknowledgements

We thank the anonymous reviewers for their critical and constructive review of the manuscript. This study was co-supported by the Fundamental Research Funds for the Central Universities, China (No. NS2021061), the Six Talent Peaks Project in Jiangsu Province, China (No. KTHY-025), the China Postdoctoral Science Foundation No. 2020M681586), the Natural Science Foundation of Jiangsu Province (No. BK20200437), the Interdisciplinary Innovation

Foundation for doctoral students of Nanjing University of Aeronautics and Astronautics (No. KXKCXJJ202008).

References

1. Bao CY, Wang P, Tang GJ. Integrated method of guidance, control and morphing for hypersonic morphing vehicle in glide phase. Chin J Aeronaut 2021;34(5):535–53.
2. Cao R, Shen HD, Liu YB, et al. The LOES-based control scheme of aerospace vehicle under flying quality constraints. Acta Astronaut 2020;177:258–69.
3. Dong CY, Liu C, Wang Q, et al. Switched adaptive active disturbance rejection control of variable structure near space vehicles based on adaptive dynamic programming. Chin J Aeronaut 2019;32(7):1684–94.
4. Chen BY, Liu YB, Shen HD, et al. Performance limitations in trajectory tracking control for air-breathing hypersonic vehicles. Chin J Aeronaut 2019;32(1):167–75.
5. Viavattene G. Flying qualities and controllability of hypersonic spaceplanes [dissertation]. Nederland: Delft University of Technology; 2018.
6. Ramnath RV. Multiple scales theory and aerospace applications. Reston: AIAA; 2010.
7. Zhu MY, Wang X, Pei XT, et al. Modified robust optimal adaptive control for flight environment simulation system with heat transfer uncertainty. Chin J Aeronaut 2021;34(2):420–31.
8. Shahzad Sana K, Hu W. Hypersonic reentry trajectory planning by using hybrid fractional-order particle swarm optimization and gravitational search algorithm. Chin J Aeronaut 2021;34(1):50–67.
9. Sushnigdha G, Joshi A. Re-entry trajectory design using pigeon inspired optimization. AIAA atmospheric flight mechanics conference. 2017 June 5-9; Denver, Colorado, USA. Reston: AIAA; 2017.
10. Yang C, Kumar M. Closed-loop adaptive Monte Carlo framework for uncertainty forecasting in nonlinear dynamic systems. J Guid Control Dyn 2019;42(6):1218–36.
11. Guo J, Li ZJ, Keyser T. A Bayesian approach for integrating multilevel priors and data for aerospace system reliability assessment. Chin J Aeronaut 2018;31(1):41–53.
12. Li BY, Zhang LG, Zhu XJ, et al. Reliability analysis based on a novel density estimation method for structures with correlations. Chin J Aeronaut 2017;30(3):1021–30.
13. Abedin F, Tralli G. Harnack inequality for a class of Kolmogorov–Fokker–Planck equations in non-divergence form. Arch Ration Mech Anal 2019;233(2):867–900.
14. Xiong FF, Chen SS, Xiong Y. Dynamic system uncertainty propagation using polynomial chaos. Chin J Aeronaut 2014;27(5):1156–70.
15. Guo JH, Lin GP, Bu XQ, et al. Sensitivity analysis of flowfield modeling parameters upon the flow structure and aerodynamics of an opposing jet over a hypersonic blunt body. Chin J Aeronaut 2020;33(1):161–75.
16. Zhao K, Guo ZD, Li Q, et al. Robust design of laminar flow supercritical airfoil based on PCE method. Chin J Appl Mech 2016;33(6):929–35,1113 [Chinese].
17. Wu XJ, Zhang WW, Song SF, et al. Sparse grid-based polynomial chaos expansion for aerodynamics of an airfoil with uncertainties. Chin J Aeronaut 2018;31(5):997–1011.
18. Manan A, Cooper J. Design of composite wings including uncertainties: a probabilistic approach. J Aircr 2009;46(2):601–7.
19. Vazquez R, Rivas D. Propagation of initial mass uncertainty in aircraft cruise flight. J Guid Control Dyn 2013;36(2):415–29.
20. Dutta P, Bhattacharya R. Nonlinear estimation of hypersonic state trajectories in Bayesian framework with polynomial chaos. J Guid Control Dyn 2010;33(6):1765–78.
21. Whittle LJ, Sagliano M. Stochastic optimal trajectory generation via multivariate polynomial Chaos. 2018 AIAA guidance, navigation, and control conference, 2018.
22. Cottrill G, Harmon F. Hybrid Gauss pseudospectral and generalized polynomial chaos algorithm to solve stochastic trajectory optimization problems. AIAA guidance, navigation, and control conference, 2011.
23. Xiong FF, Xiong Y, Xue B. Trajectory optimization under uncertainty based on polynomial chaos expansion. AIAA guidance, navigation, and control conference, 2015.
24. Yu ZS, Zhao ZD, Cui PY. An observability-based trajectory optimization considering disturbance for atmospheric entry. AIAA guidance, navigation, and control conference, 2016.
25. Li X, Nair PB, Zhang ZG, et al. Aircraft robust trajectory optimization using nonintrusive polynomial chaos. J Aircr 2014;51(5):1592–603.
26. Jones BA, Doostan A, Born GH. Nonlinear propagation of orbit uncertainty using non-intrusive polynomial chaos. J Guid Control Dyn 2013;36(2):430–44.
27. Jin K, Geller DK, Luo JJ. Robust trajectory design for rendezvous and proximity operations with uncertainties. J Guid Control Dyn 2020;43(4):741–53.
28. Yang Z, Luo YZ, Zhang J. Robust planning of nonlinear rendezvous with uncertainty. J Guid Control Dyn 2017;40(8):1954–67.
29. Grant MJ, Bolender MA. Rapid, robust trajectory design using indirect optimization methods. AIAA atmospheric flight mechanics conference, 2015.
30. Flanzer T, Bower G, Kroo I. Robust trajectory optimization for dynamic Soaring. AIAA guidance, navigation, and control conference, 2012.
31. Richter M, Holzapfel F. Robust noise optimal approach trajectories. AIAA guidance, navigation, and control (GNC) conference, 2013.
32. Banerjee S. Flight parameter analysis of an L1 adaptive controller of a hypersonic glider. J Aircr 2019;56(3):1149–63.
33. Murillo OJ. A fast ascent trajectory optimization method for hypersonic air-breathing vehicles [disseration]. Ames: Iowa State University; 2010.
34. Brocanelli M, Gunbatar Y, Serrani A, et al. Robust control for unstart recovery in hypersonic vehicles. AIAA guidance, navigation, and control conference;, 2012.
35. Chang JT, Fan Y, Bao W, et al. Unstart margin control of hypersonic inlets. Acta Astronaut 2010;66(1-2):78–87.
36. Aeronautical-Systems-Center, Wright Patterson-AFB Ohio. Flying qualities of piloted airplanes MIL-F-1797A. Washington, D.C.: U.S. Dept. of Defense; 2004.
37. Cao R, Shen HD, Liu YB, et al. Robust optimization of commands based on polynomial chaos and application in flight control. Control Theory Appl 2020;37(12):2482–92 [Chinese].
38. Wang FG, Xiong FF, Jiang H, et al. An enhanced data-driven polynomial chaos method for uncertainty propagation. Eng Optim 2018;50(2):273–92.
39. Nouy A, Le Maître OP. Generalized spectral decomposition for stochastic nonlinear problems. J Comput Phys 2009;228(1):202–35.
40. Gerritsma M, van der Steen JB, Vos P, et al. Time-dependent generalized polynomial chaos. J Comput Phys 2010;229(22):8333–63.
41. Kolmogorov AN. Foundations of the theory of probability. second edition. New York: Dover Publications; 2018. p. 6–13.
42. Prempraneerach P, Hover FS, Triantafyllou MS, et al. Uncertainty quantification in simulations of power systems: Multi-element polynomial chaos methods. Reliab Eng Syst Saf 2010;95(6):632–46.
43. Serrani A, Bolender MA. Addressing limits of operability of the scramjet engine in adaptive control of a generic hypersonic vehicle. 2016 IEEE 55th conference on decision and control. 2016 December 12-14; Las Vegas, USA. Piscataway: IEEE Press; 2016. p. 7567–72.